

# Efficiency limits of electronically coupled upconverter and quantum ratchet solar cells using detailed balance

Emily Z. Zhang<sup>1, a)</sup> and Jacob J. Krich<sup>1, 2, b)</sup>

<sup>1)</sup>*Department of Physics, University of Ottawa, Ottawa, ON, Canada*

<sup>2)</sup>*School of Electrical Engineering and Computer Science, University of Ottawa, Ottawa, ON, Canada*

The intermediate band solar cell (IBSC) and quantum ratchet solar cell (QRSC) have the potential to surpass the efficiency of standard single-junction solar cells by allowing sub-gap photon absorption through states deep inside the band gap. High efficiency IBSC and QRSC devices have not yet been achieved, however, since introducing mid-gap states also increases recombination, which can harm the device. We consider the electronically coupled upconverter (ECUC) solar cell and show that it can achieve the same efficiencies as the QRSC. Although they are equivalent in the detailed balance limit, the ECUC design was proposed in order to be less sensitive to nonradiative processes, which makes it a more practical implementation for IB devices. We perform a case study of crystalline-silicon based ECUC cells, focusing on hydrogenated amorphous silicon as the upconverter material and highlighting potential dopants for the ECUC. These results illustrate a new path for the development of IB-based devices.

## I. INTRODUCTION

Shockley and Queisser used the detailed balance (DB) formalism to show that the efficiency of a solar cell made from a semiconductor with a single band gap and standard carrier thermalization can never exceed 31% under unconcentrated black-body sunlight.<sup>1</sup> Intermediate band (IB) materials – semiconductors with allowed electronic states deep in the gap, as shown in Figure 1a – enable solar cells to break this limit by absorbing sub-gap photons with a voltage limited by the large band gap.<sup>2</sup> In the radiative limit, the maximum efficiency of an intermediate band solar cell (IBSC) at one sun concentration is 46.8%, significantly exceeding the Shockley-Queisser limit.<sup>2</sup> Several intermediate band devices have been demonstrated in quantum dot, highly mismatched alloy, organic, perovskite, and doped semiconductor systems,<sup>3–10</sup> but high efficiencies have not been realized due to nonradiative recombination, low subgap absorption, or both.<sup>11</sup>

The quantum ratchet (QR) solar cell has been proposed as an improved implementation of the IBSC.<sup>12</sup> The intermediate band QR and conduction band QR implementations are shown in Figure 1b-c, respectively. The original idea of an IBQR solar cell was to increase the lifetime of carriers in the IB. In the case of the IBQR, carriers relax from the IB to a ratchet band (RB), which can suppress recombination to the valence band (VB). The ratchet also enables improved voltage matching between the subgap transitions and the band-to-band transitions.<sup>13,14</sup> The CBQR has the ratchet step above the conduction band edge, and an analogous valence band QR (not shown) has the ratchet step below the valence band edge. All three QR designs realize the voltage-matching improvements and can achieve detailed balance maximum efficiencies of 48.5% at one sun, greater than that of IBSCs.<sup>12</sup> There have, however, been few QR experimental realizations, and there are few suggestions for material systems.<sup>15</sup>

In both IBSC and QRSC devices, the IB and QR regions are added to *pn* junctions made of standard semiconductors (i.e., without intermediate bands) in hopes of increasing current in the device, but short nonradiative lifetimes of electrons and holes in the IB region can severely reduce device efficiency. Both IBSCs and QRSCs have an *n*-IB-*p* architecture, implying the holes created at the front of the cell must travel through the IB region to be collected. If hole nonradiative lifetimes in the IB or QR regions are short, the nonradiative losses in the IB region will exceed the extra current generation, making efficiencies less than for the *pn*-diode solar cell alone in the absence of the IB region.<sup>16,17</sup>

The electronically coupled upconverter (ECUC) is a less-studied architecture, originally proposed to provide the efficiency of an IBSC while being less sensitive to nonradiative processes.<sup>18,19</sup> It is named in analogy to optical upconverters, which can be placed behind the cell, where they absorb subgap photons that pass through the cell and then emit higher-energy photons, which can be reabsorbed in the cell. Such optical upconverters have an unconcentrated detailed balance efficiency limit of 47.6%, close to the IBSC and QRSC.<sup>20</sup> Similar to an optical upconverter, the ECUC absorbs subgap photons at the rear of the device, but it injects the higher energy carriers (electrons or holes) directly into the standard semiconductor rather than emitting a higher-energy photon. Figure 1d shows one instantiation of the ECUC with an *n*-*p*-IB structure, where the material with an IB with energy  $E_I$  is placed at the back of the device and can have a different band gap  $E_{g2}$  than in the standard semiconductor,  $E_{g1}$ , unlike in the IBSC and QRSC, where the large band gap  $E_{CV}$  is generally considered to be uniform through the device. In Figure 1d, the ECUC is shown with no valence band offset, but other configurations are also possible, including an equivalent design with no conduction band offset, in a *p*-*n*-IB structure.

As with IBSC, QRSC, and optical upconverters, the ECUC allows absorption of subgap photons, with the difference being how the resulting carriers are electrically injected into the standard semiconductor. The minority carriers produced by absorption in the *pn* junction never transit the IB region, so the current added from IB absorption can be obtained strictly as

<sup>a)</sup>Current address: Department of Physics, University of Toronto, Toronto, ON, Canada

<sup>b)</sup>Electronic mail: jkrich@uottawa.ca

This is the author's peer reviewed, accepted manuscript. However, the online version of record will be different from this version once it has been copyedited and typeset.  
PLEASE CITE THIS ARTICLE AS DOI: 10.1063/1.50005416

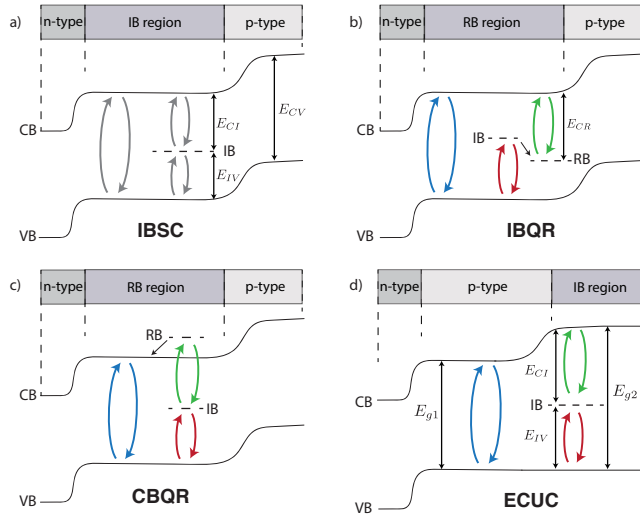


FIG. 1. Example band diagrams of (a) intermediate band solar cell, (b) intermediate band quantum ratchet, (c) conduction band quantum ratchet, and (d) electronically coupled upconverter (ECUC) devices. The red, green, and blue processes for the ratchets and ECUC are equivalent in detailed balance.

an addition, and low quality (i.e., short nonradiative lifetime) upconverter material cannot harm the cell in the same way as in the IBSC/QRSC.<sup>18,19</sup> However, the ECUC requires more complicated 2D contacts to avoid extracting current from the IB, with one possibility shown in Figure 2.

The detailed balance limiting efficiencies for the ECUC have not previously been calculated. In this work, we focus on the radiative limit and demonstrate that the ECUC design can exceed the efficiency of an IBSC and is mathematically equivalent to the QRSC in the DB limit. We show that, as with the QRSC, the ECUC configuration has the potential to exceed IBSC efficiencies at solar concentrations up to 23,000 suns. At higher concentrations, we show that an ECUC with  $E_{g2} < E_{g1}$  (mathematically equivalent to a QRSC with a negative ratchet step) can exceed the maximum IBSC efficiency at full concentration, albeit by only 0.02% (absolute). This negative ratchet has not been previously considered. We perform a global optimization showing the maximum efficiencies possible as functions of  $E_{g1}$  and  $E_{g2}$  at 1-sun and full concentration and also consider a case study of an ECUC based on crystalline silicon (c-Si), the most widely used and studied PV material. We show that there is potential to improve on c-Si solar cells using an ECUC.

## II. DETAILED BALANCE MODEL

We use the well-known detailed balance formalism to model the ECUC and QRSC. We first show that in detailed balance the ECUC and QRSC are mathematically equivalent, then we compute the limiting efficiencies for ECUC.

Detailed balance calculations assume all recombination is radiative, carriers have infinite mobility, each absorbed pho-

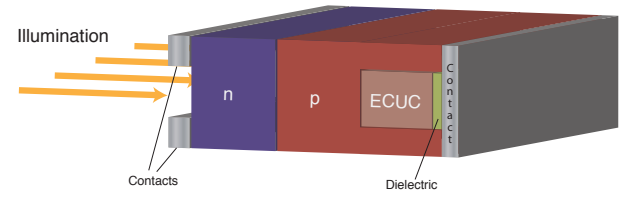


FIG. 2. Schematic of a potential device architecture for the ECUC allowing extraction of both electrons and holes from the ECUC to the host p-type semiconductor without extraction of intermediate band carriers.

ton produces only one electron-hole pair, and the cell is thick enough to assure full absorption of photons for each allowable transition. We further assume perfect photon selectivity, with each photon energy absorbed by only one transition; this condition is called non-overlapping absorptions and is not required for detailed balance.<sup>2,21,22</sup> We make the standard assumption that electrons are collected at one side of the device and holes at the other; a  $pn$  junction is one way to effect this separation of carriers,<sup>1</sup> as depicted in Fig. 1, but carrier-selective contacts could be used instead. Since the carriers have infinite mobility,

$$\mu_{CV} = qV_{\text{ext}}, \quad (1)$$

where  $q$  is the elementary charge,  $\mu_{CV}$  is the quasi-Fermi level difference between the electrons and holes, and  $V_{\text{ext}}$  is the external voltage. We choose units with  $q = 1$ .

Another key assumption is that there is one electron-hole pair generated/lost for each photon absorbed/emitted. Since all recombination events are assumed to be radiative, this assumption implies that the current in the device must equal the difference between the photon fluxes  $\phi$  in and out of the device. These fluxes obey the modified Planck spectrum<sup>23</sup>

$$\begin{aligned} \phi(E_{\min,AB}, E_{\max,AB}, T, \mu_{AB}) \\ = \frac{2F}{h^3 c^2} \int_{E_{\min,AB}}^{E_{\max,AB}} \frac{E^2 dE}{e^{(E-\mu_{AB})/kT} - 1}, \end{aligned} \quad (2)$$

where the process between bands  $A$  and  $B$  absorbs photons with energies between  $E_{\min,AB}$  and  $E_{\max,AB}$ ,  $T$  is the temperature,  $\mu_{AB}$  is the chemical potential difference between carriers in bands  $A$  and  $B$ ,  $h$  is Planck's constant,  $c$  is the speed of light,  $k$  is Boltzmann's constant, and  $F$  is the geometrical factor denoting the fraction of light incident on the cell. For the sun,  $F_{\text{sun}} = X f_s$  where  $X$  is the solar concentration factor and

$$f_s = \pi \left( \frac{\text{radius of sun}}{\text{distance between earth and sun}} \right)^2. \quad (3)$$

For emission from the cell,  $F_{\text{cell}} = \pi$ .

In detailed balance, we have two photon sources: the sun and the cell. We denote the photons absorbed from the sun in transitions between bands  $A, B$  by

$$\dot{N}_{AB}^{\text{sun}} = \phi(E_{\min,AB}, E_{\max,AB}, T_s, 0), \quad (4)$$

and the photons emitted by the cell in transitions between bands  $A, B$  by

$$\dot{N}_{AB}^{\text{cell}} = \phi(E_{\min,AB}, E_{\max,AB}, T_a, \mu_{AB}), \quad (5)$$

where  $T_s$  is the solar radiation temperature, which we take to be 6000 K, and  $T_a$  is the ambient temperature, which we take to be 300 K. The current extracted from band  $A$  is the difference between absorbed and emitted photons involving band  $A$ ,

$$J_A = \sum_B \pm (\dot{N}_{AB}^{\text{sun}} - \dot{N}_{AB}^{\text{cell}}(\mu_{AB})), \quad (6)$$

with the sign depending on whether the  $AB$  absorption process creates (+) or destroys (−) carriers in band  $A$ .

For all of the devices, the total current is the net current extracted from either the CB or the VB, which are equal. For an ECUC, the total current is

$$J_C^{\text{ECUC}} = \dot{N}_{CV}^{\text{sun}} - \dot{N}_{CV}^{\text{cell}}(\mu_{CV}) + \dot{N}_{CI}^{\text{sun}} - \dot{N}_{CI}^{\text{cell}}(\mu_{CI}). \quad (7)$$

We also assume that no current is extracted from the intermediate band, so

$$J_I^{\text{ECUC}} = 0 = \dot{N}_{IV}^{\text{sun}} - \dot{N}_{IV}^{\text{cell}}(\mu_{IV}) - \dot{N}_{CI}^{\text{sun}} + \dot{N}_{CI}^{\text{cell}}(\mu_{CI}). \quad (8)$$

Note that the CI processes in Eq. 8 enter with opposite signs from Eq. 7, as optical absorption from IB to CB removes an IB carrier. Detailed balance calculations often make the non-overlapping absorption assumption that a photon with energy  $E$  can be absorbed only by the highest energy transition permitted by conservation of energy.<sup>2</sup> Then all photons with energy greater than  $E_{g1}$  contribute to the CV transition; the  $\dot{N}_{CV}$  terms have energy range  $[E_{g1}, \infty]$ . When  $E_{IV} < E_{g2}/2$ , the  $\dot{N}_{IV}$  terms have energy range  $[E_{IV}, E_{CI}]$  and the  $\dot{N}_{CI}$  terms have energy range  $[E_{CI}, E_{g1}]$ . The upper bound for the  $\dot{N}_{CI}$  terms is  $E_{g1}$  instead of  $E_{g2}$  as a result of the absorption being perfectly non-overlapping; due to this assumption, photons with energies between  $E_{g1}$  and  $E_{g2}$  (when  $E_{g2} > E_{g1}$ ) are included in the CV transition, spatially located in the  $pn$ -junction. When  $E_{IV} > E_{g2}/2$ , the IV and CI optical thresholds are rearranged accordingly; the current remains unchanged if  $E_{IV}$  is reflected around  $E_{g2}/2$ , replacing  $E_{IV}$  with  $E_{g2} - E_{IV}$ .

Though the primary purpose of the ECUC architecture is to have  $E_{g2} > E_{g1}$ , as drawn in Fig. 1, we also consider the somewhat surprising case of  $E_{g2} < E_{g1}$ . In that situation, we continue to use the energy ranges described just above, even though those energy ranges give photons with energy between  $E_{g2}$  and  $E_{g1}$  to the CI transition (or to the IV transition, if  $E_{IV} > E_{g2}/2$ ) instead of to the higher-energy CV transition in the upconverter. We discuss this choice and its result, giving the highest efficiency at full concentration, at the end of this section.

With equations 1, 7, 8, and the fact that

$$\mu_{CV} = \mu_{CI} + \mu_{IV}, \quad (9)$$

we can solve for the chemical potentials and compute  $J(V)$ . These equations are of the same form as in the original IBSC

calculation,<sup>2</sup> but the ECUC has different energy thresholds associated with the various terms.

For an IBQR, we assume the carriers in the IB and RB share a common quasi-Fermi level, so  $\mu_{CI} = \mu_{CR}$ .<sup>12</sup> Then, the net current from the CB and IB are

$$J_C^{\text{IBQR}} = \dot{N}_{CV}^{\text{sun}} - \dot{N}_{CV}^{\text{cell}}(\mu_{CV}) + \dot{N}_{CR}^{\text{sun}} - \dot{N}_{CR}^{\text{cell}}(\mu_{CR}), \quad (10)$$

$$J_I^{\text{IBQR}} = 0 = \dot{N}_{IV}^{\text{sun}} - \dot{N}_{IV}^{\text{cell}}(\mu_{IV}) - \dot{N}_{CR}^{\text{sun}} + \dot{N}_{CR}^{\text{cell}}(\mu_{CR}). \quad (11)$$

These have similar form to Eqs. 7, 8 but with different energy ranges. The  $\dot{N}_{CV}$  terms have energy range  $[E_{CV}, \infty]$ . When  $E_{IV} < E_{CV}/2$ , the  $\dot{N}_{IV}$  terms have energy range  $[E_{IV}, E_{CR}]$ , and the  $\dot{N}_{CR}$  terms have energy range  $[E_{CR}, E_{CV}]$ . When  $E_{IV} > E_{CV}/2$ , the IV and CR optical thresholds are rearranged accordingly.

These equations for the ECUC and IBQR are equivalent. As shown in Figure 1d,  $E_{CI} + E_{IV} = E_{g2}$  for the ECUC. If we choose  $E_{CV}$  for the IBQR to equal  $E_{g1}$  for the ECUC, then the first two terms in each of Eqs. 10 and 11 are equal to the equivalent terms in Eqs. 7 and 8. Further, if  $E_{CR}$  for the IBQR equals  $E_{CI}$  for the ECUC, and  $E_{IV} + E_{CR}$  for the IBQR equals  $E_{g2}$  for the ECUC, then the last two terms in each of those equations become equivalent. Therefore the ECUC equations are equal to the IBQR equations. Similarly, if  $E_{IV} + E_{RI} = E_{g2}$  for the CBQR or  $E_{IR} + E_{CI} = E_{g2}$  for the valence band QR, then the equations also become equivalent to the ECUC. Since the equations for QR and ECUC are no different in detailed balance, the limiting efficiencies are also the same.

Figure 3 shows the maximum ECUC efficiencies at  $X = 1$  and  $X = 1/f_s = 46200$ , which is the maximum value. The peak efficiencies and band gaps for these cases are shown in Table I. The diagonal at  $E_{g1} = E_{g2}$  represents standard IB solar cells, and at one sun concentration (top), the detailed balance efficiency is highest at  $E_{g2} > E_{g1}$ . This result indicates that the ECUC has higher limiting efficiency than IBSC, similar to QR,<sup>12</sup> spectrally selective reflectors,<sup>24</sup> and overlapping absorptions.<sup>21</sup> Therefore, the ECUC can exceed both the Shockley-Queisser and IBSC limits. Figure 3 shows that there is a wide range of band gaps that can potentially achieve this goal.

At full concentration, both the ECUC and the IBSC significantly exceed the single junction efficiency limit, which has motivated interest in combining IBSC with concentrator systems.<sup>25,26</sup> It has long been found that under full concentration, the IBSC ( $E_{g2} = E_{g1}$ ) is the optimal structure,<sup>12,21,24</sup> but we show that the actual optimum efficiency occurs in the previously unconsidered situation with  $E_{g2} < E_{g1}$ , though the efficiency gain by moving to the optimal configuration of  $E_{g1} - E_{g2} = 15$  meV is only 0.02% (absolute).

Figure 4 shows the evolution of the maximum efficiency ECUC cell as a function of  $X$ , showing that the ECUC configuration with  $E_{g2} > E_{g1}$  is optimal for  $X < 23,000$ , and that  $E_{g2}$  close to  $E_{g1}$ , as in an IBSC, is optimal for  $X > 23,000$ . The origins of the improved efficiency of a ratchet system at lower concentrations have been described in terms of entropy reduction<sup>12</sup> and voltage matching,<sup>14</sup> but their evolution with  $X$  has not previously been detailed. We think about the trade-off as being between voltage matching and current loss. The

This is the author's peer reviewed, accepted manuscript. However, the online version of record will be different from this version once it has been copyedited and typeset.  
PLEASE CITE THIS ARTICLE AS DOI: 10.1063/5.0005416

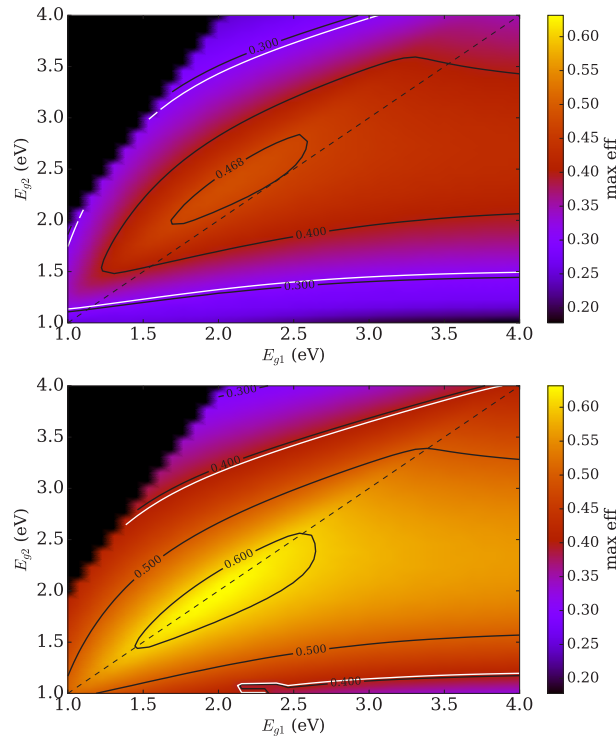


FIG. 3. Maximum ECUC efficiency in detailed balance, with optimized  $E_I$ , at 1 sun concentration (top) and at full concentration ( $X = 46200$ ) (bottom). The Shockley-Queisser limits of 31% ( $X = 1$ ) and 40.7% ( $X = 46200$ ) are shown with the white contours. Note that an ECUC can only be beneficial if  $E_{g2} \leq 2E_{g1}$ , since both sub-gap transitions must have energy thresholds below  $E_{g1}$ . The dashed line along the diagonal shows  $E_{g1} = E_{g2}$ , the IBSC limit.

TABLE I. Maximum efficiency parameters with a blackbody spectrum at 1 sun and full concentration. Note that there is a symmetry when  $E_{IV}$  is replaced by  $E_{g2} - E_{IV}$ ; we take the larger values for  $E_{IV}$ .

System	$X$	$E_{g1}$ (eV)	$E_{g2}$ (eV)	$E_{IV}$ (eV)	Efficiency
Single-junction	1	1.31	-	-	30.96%
IB solar cell	1	2.42	-	1.49	46.77%
ECUC solar cell	1	2.09	2.36	1.42	48.47%
Single-junction	46200	1.11	-	-	40.74%
IB solar cell	46200	1.95	-	1.24	63.17%
ECUC solar cell	46200	1.96	1.95	1.24	63.19%

full solution of the DB equations shows the effect, but we can understand the key physics with a simplified model. Consider that we have concentration  $X$  and that  $E_{g1} = E_{g2}$  (i.e., in the IBSC limit) with  $E_{IV}$  and voltage  $V$  chosen to be near optimal. The power from the cell is  $P = VJ(V)$ , and we want to know the sign of  $\partial P / \partial E_{g2} |_{E_{g2}=E_{g1}}$ , which describes whether it is valuable to produce a ratchet. Without loss of generality, we examine the case with  $E_{IV} > E_{g1}/2$ . We can simplify the full model of Eqs. 7-9 by taking the Boltzmann approximation (i.e., ignoring the “-1” in the denominator of Eq. 2 at

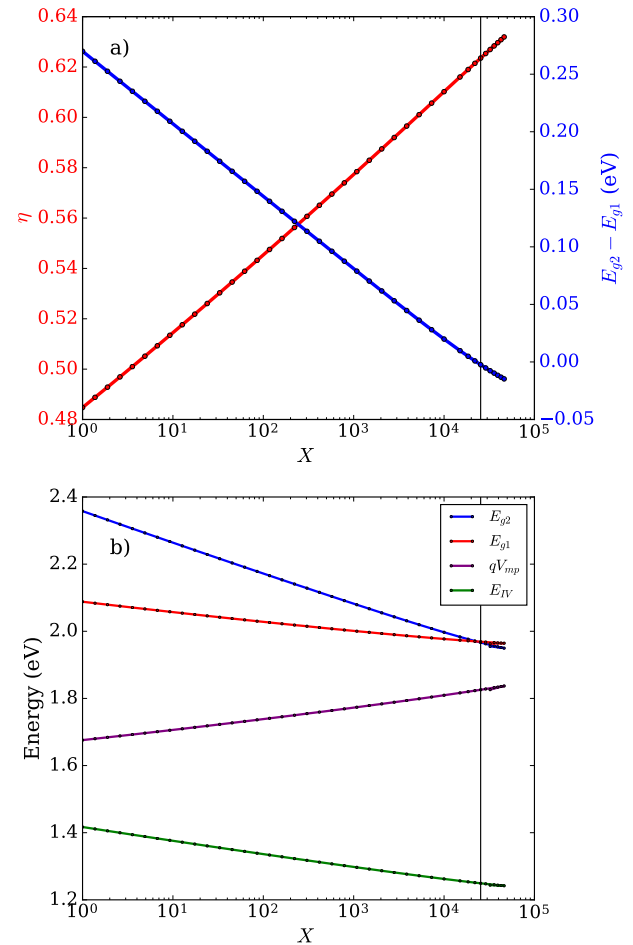


FIG. 4. (a) Maximum efficiency (red line, left axis) and optimized value of  $E_{g1} - E_{g2}$  (blue line, right axis) for an ECUC as a function of solar concentration  $X$ . Thin vertical line shows the transition point, above which a ratchet design no longer improves on a standard IBSC. (b) Optimal values of  $E_{g2}$ ,  $E_{g1}$ ,  $E_{IV}$  and  $qV_{mp}$  at each  $X$ .

temperature  $T_a$ ), giving

$$\dot{N}_{AB}^{\text{cell}} \approx R_{AB}^0 e^{\mu_{AB}/kT_a} \quad (12)$$

$$R_{CI}^0 = \frac{2\pi}{h^3 c^2} \int_{E_{g2}-E_{IV}}^{E_{IV}} E^2 e^{-E/kT_a} \quad (13)$$

$$R_{IV}^0 = \frac{2\pi}{h^3 c^2} \int_{E_{IV}}^{E_{g1}} E^2 e^{-E/kT_a} \quad (14)$$

$$R_{CV}^0 = \frac{2\pi}{h^3 c^2} \int_{E_{g1}}^{\infty} E^2 e^{-E/kT_a}. \quad (15)$$

In this approximation, Eq. 8 can be solved explicitly for  $e^{\mu_{CI}/kT_a}$  and then plugged into Eq. 7 to give the Strandberg form<sup>27</sup>

$$J = \dot{N}_{CV}^{\text{sun}} - R_{CV}^0 e^{V/kT_a} + \frac{\dot{N}_{IV}^{\text{sun}} + \dot{N}_{CI}^{\text{sun}}}{2} - \sqrt{R_{IV}^0 R_{CI}^0 e^{V/kT_a} + \left( \frac{\dot{N}_{IV}^{\text{sun}} - \dot{N}_{CI}^{\text{sun}}}{2} \right)^2}. \quad (16)$$

Optimal efficiency requires that the system be close to current matched in the subgap transitions,  $\dot{N}_{CI}^{\text{sun}} \approx \dot{N}_{IV}^{\text{sun}}$ . The derivation is simpler if we assume that this condition holds exactly. Note that in Eq. 16, only  $\dot{N}_{CI}^{\text{sun}}$  and  $R_{CI}^0$  depend on  $E_{g2}$ . Then in the current matching limit, it is simple to evaluate

$$\begin{aligned} \frac{\partial P}{\partial E_{g2}} &= V \left( \frac{1}{2} \frac{\partial \dot{N}_{CI}^{\text{sun}}}{\partial E_{g2}} - \frac{1}{2} \sqrt{\frac{R_{IV}^0 e^{V/kT_a}}{R_{CI}^0}} \frac{\partial R_{CI}^0}{\partial E_{g2}} \right) \\ &= \frac{V}{2} \frac{\pi}{h^3 c^2} (E_{g2} - E_{IV})^2 \left( \frac{-f_s X}{e^{(E_{g2} - E_{IV})/kT_s} - 1} \right. \\ &\quad \left. + e^{-(E_{g2} - E_{IV})/kT_a} \sqrt{\frac{R_{IV}^0 e^{V/kT_a}}{R_{CI}^0}} \right) \end{aligned} \quad (17)$$

The first term in Eq. 17 gives the current loss to the CI process as the ratchet increases, giving a negative contribution to power, and is proportional to  $X$ . The second term is the positive change due to improved voltage matching, which originates in the decrease of the radiative recombination parameter  $R_{CI}^0$ . At small  $X$ , the voltage matching term is more important, and  $P$  increases with  $E_{g2}$ . At larger  $X$ , the current loss begins to dominate, and the critical value of  $X$  at which  $E_{g1} = E_{g2}$  becomes optimal can be found by setting Eq. 17 equal to 0. Using the exact results from Fig. 4(b), we can evaluate the sign of  $\partial P / \partial E_{g2}$  near the optimal choices, using  $E_{g2} = E_{g1} \approx 1.95$  eV,  $E_{IV} \approx 0.7$  eV, and  $V \approx 1.8$  eV. With those values, Eq. 17 equals zero when  $X \approx 1.2 \times 10^4$ , which is close to the exact critical value of  $X_c = 2.3 \times 10^4$ .

This simple argument is not intended to quantitatively reproduce the correct answer but rather to make clearer the origin of this effect. For  $X < X_c$ , ratchet/upconversion systems can improve over the efficiency of an IBSC. Note that since Eq. 17 is linear in  $X$ , this argument implies that for  $X > X_c$ , the efficiency should be improved by setting  $E_{g2} < E_{g1}$ , which allows more current to be absorbed, with a cost in voltage. We find precisely this result to be true, with a small efficiency improvement possible at high concentration by setting  $E_{g2} < E_{g1}$ , as shown in Fig. 4.

This slightly improved efficiency occurs with the energy cutoffs for each absorption process as described below Eq. 8, which become nonstandard when  $E_{g2} < E_{g1}$ . In particular, photons with energy between  $E_{g2}$  and  $E_{g1}$  are absorbed by the IV transition even though they could (energetically) be absorbed by the higher energy CV transition in the ECUC. This transfer of photons from the higher-energy CV transition to the lower-energy IV transition is beneficial because, at full concentration, voltage matching is improved by *increasing* the subgap currents, which is opposite to the low-concentration case. Physically realizing such a system would require having an IB material with IV subgap optical absorption coefficient much larger than the CV optical absorption coefficient for photons with energy between  $E_{g2}$  and  $E_{g1}$ . We are not familiar with any such materials.

Even when  $E_{g2}$  is significantly less than  $E_{g1}$ , current can still be extracted from an ECUC, as long as the VB and CB edges of the ECUC are at higher energies than the VB and CB edges of the p-type semiconductor, respectively, in Fig. 1d.

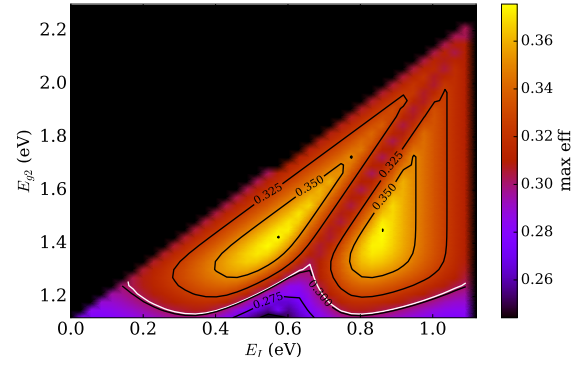


FIG. 5. Maximum ECUC efficiency in detailed balance, with  $E_{g1} = 1.12$  eV as a function of  $E_{g2}$  and  $E_I$  at 1 sun concentration. The detailed balance efficiency limit for  $E_g = 1.12$  eV is shown with the white contour. Note that the data cutoff at the diagonal (black) occurs because the ECUC requires  $E_I > E_{g2} - E_{g1}$ .

With this band alignment, holes flow to the right and electrons to the left, where carrier selective contacts permit the functioning ECUC. The voltage is limited to be no larger than the smaller of  $E_{g2}$  and  $E_{g1}$ , so energy is always conserved.

### III. CASE STUDY: ECUC USING C-SI

In this section, we perform a case study of a potential ECUC using silicon as the front  $pn$ -diode material, since c-Si is an extremely well-understood material. Adding only an intermediate band to an  $n$ -IB- $p$  c-Si solar cell actually harms the efficiency of the cell, even in the detailed balance limit.<sup>21</sup> That failure occurs due to silicon's small band gap and the assumption of non-overlapping absorptions. Figure 3, however, shows that even with  $E_{g1}$  equal to the band gap of c-Si, 1.12 eV, the ECUC allows considerable improvement over the Shockley-Queisser limit. First, we study the optimal range for  $E_{g2}$  for an ECUC on silicon. Second, we consider an ECUC made of hydrogenated amorphous silicon (a-Si), which is a higher band-gap material frequently used for heterojunctions with c-Si. We perform a search for the best-suited  $E_I$  for an a-Si upconverter on c-Si.

Figure 5 shows the maximum ECUC efficiency with  $E_{g1} = 1.12$  eV as a function of  $E_{g2}$  and  $E_I$ . The peak efficiencies and band gaps are shown in Table II. The optimal range of  $E_{g2}$  lies approximately between 1.3 and 1.6 eV, with the maximum efficiency at  $E_{g2} = 1.47$  eV, with  $E_I$  near 0.9 eV. As  $E_{g2}$  approaches  $E_{g1}$ , we recover the IBSC efficiency, which is lower than the Shockley-Queisser limit for a device with  $E_g = 1.12$  eV. Note that when  $E_{g2} > 1.3$  eV, the ECUC improves efficiencies for all values of  $E_I$ . For a large range of band gaps, it is possible to significantly exceed the SQ limit; therefore, there is potential for high efficiency silicon devices if an ECUC is added.

A promising upconverter material is amorphous silicon, since its band gap of  $E_{g2} = 1.55$  eV falls in the high-efficiency

This is the author's peer reviewed, accepted manuscript. However, the online version of record will be different from this version once it has been copyedited and typeset.  
PLEASE CITE THIS ARTICLE AS DOI: 10.1063/1.50005416

TABLE II. Maximum detailed balance efficiencies for c-Si ( $E_g = 1.12$  eV) at 1 sun concentration. Note that there is a symmetry for  $E_I \leftrightarrow E_{g2} - E_I$ ; we take the larger values for  $E_I$ .

System	$E_{g1}$ (eV)	$E_{g2}$ (eV)	$E_I$ (eV)	Efficiency
Single junction	1.12	-	-	30.2%
IB solar cell	1.12	-	0.85	29.7%
ECUC solar cell	1.12	1.47	0.86	37.4%

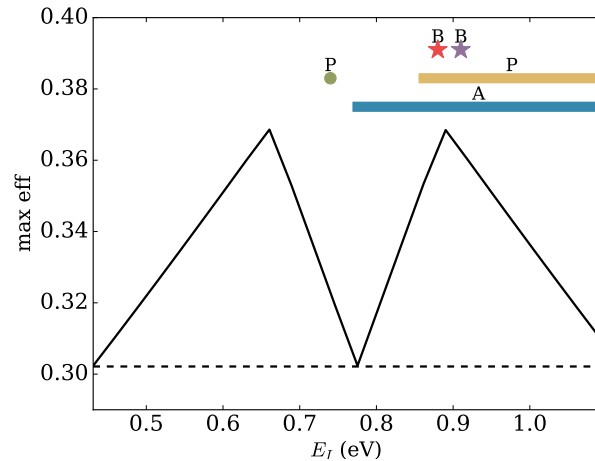


FIG. 6. Maximum ECUC efficiency vs.  $E_I$  for c-Si ( $E_{g1} = 1.12$  eV) and an a-Si upconverter ( $E_{g2} = 1.55$  eV). The black dashed line shows the single-junction detailed balance efficiency with  $E_g = 1.12$  eV. The potential dopants are labelled at their respective  $E_I$ . Doping with P is shown with the green dot (optical<sup>31</sup>) and a range of values with the yellow line (electrical activation<sup>32</sup>). Thermal activation energies for B are shown with stars, with red corresponding to doping with  $\text{BF}_3$ <sup>33</sup> and purple to  $\text{B}_2\text{H}_6$ .<sup>31</sup> The blue line shows the range of  $E_I$  from thermal activation for alkali dopants, including Na, K, Rb, and Cs.<sup>34</sup>

range,<sup>28</sup> and a-Si on c-Si devices are routinely made.<sup>29</sup> Figure 6 shows DB efficiency as a function of  $E_I$  of an ideal radiatively limited device using the band gaps of c-Si with an a-Si ECUC. A real device will not achieve this radiative limit, but as with all detailed balance limits, it shows the potential of the architecture. All values of  $E_I$  between  $E_{g2} - E_{g1} = 0.43$  eV and  $E_{g1} = 1.12$  eV give improved efficiencies over the bare c-Si cell. Doping of a-Si is more complicated than in crystalline semiconductors, as dopants can induce local coordination changes and dangling bonds, and the structures vary depending on deposition method.<sup>30</sup> The resulting  $E_I$  for a dopant in a-Si can thus vary considerably depending on a-Si deposition and dopant precursor and pressure.<sup>30</sup> This variation could allow tuning of ECUC energy levels, which is not generally possible in crystalline semiconductor:dopant materials. To date, devices based on doped a-Si have generally desired shallow dopants, as in c-Si, so the most-studied dopants are those that produce relatively shallow states in the band gap, to give high conductivities. For an ECUC, optically active midgap states are desirable, which is the opposite of the standard case.

Figure 6 also shows estimated energetic positions for some

common dopants in a-Si. The most studied dopants include boron and phosphorus as acceptors and donors, respectively, as in c-Si. Even when a-Si has tetrahedrally coordinated silicon, the bond angle distortions tend to make dopant energy levels lie deeper in the gap than in c-Si.<sup>35</sup> As an acceptor, B doping using  $\text{B}_2\text{H}_6$  or  $\text{BF}_3$  gives an electrical activation energy of  $E_I = 0.88 - 0.91$  eV, with a higher concentration of active dopant states formed from the  $\text{BF}_3$  precursor.<sup>31,33</sup> As a donor, P doping using  $\text{PH}_3$  gives optical absorption in a band around  $E_{g2} - E_I = 0.81$  eV.<sup>31</sup> As can be seen in Fig. 6, this energy level appears close to the middle of the band gap, which allows only minimal improvement in these detailed balance calculations. The dip in efficiency for  $E_I \approx E_{g2}/2$  is an artifact of the non-overlapping absorption condition, as one of the subgap transitions becomes artificially depleted of photons when  $E_I$  is close to mid-gap. Removing the non-overlapping absorption requirement, which is only a simplification for theoretical analysis, reduces the penalty for cells with IB's at mid-gap,<sup>21,22</sup> so this mid-gap  $E_I$  can still be beneficial for the ECUC. Doping with P has also been shown to produce thermal activation energies ranging from 0.74 eV to 0.27 eV, depending on concentration of the precursor, with higher activation energies at lower doping concentrations.<sup>32</sup> Alkali atoms as donors, including Na, K, Rb, and Cs, have been shown to produce thermal activation energies that are similar to each other, ranging from 0.80 eV to 0.20 eV, again with higher activation energies at lower dopant concentrations.<sup>34</sup> We interpret these activation energies to be  $E_{g2} - E_I$ . These values contain overlap with the optimal efficiency range for a c-Si/a-Si ECUC. A working ECUC must be optically thick for the subgap photons, which requires either a high dopant concentration or a thick absorber layer. If high dopant concentration is required, the alkali dopant energy levels may be less than than  $E_{g2} - E_{g1}$  and thus outside of the useful energy range.

A functioning ECUC requires that the IB states be partially filled during device operation, as for the IBSC.<sup>2</sup> Such partial filling can be obtained either by partial compensation of the deep-level dopants or by photofilling.

The combination of c-Si and a-Si has great potential to make a working ECUC that can improve the efficiency of c-Si solar cells. To realize this potential, the energetic position of those defect states and their optical properties must be characterized, both for the common electrical dopants and possibly a much larger range of potential IB-forming dopants. A wide array of dopant elements may be interesting for a-Si based ECUC, just as a wide array of dopants may be useful for c-Si based IBSC's.<sup>36</sup>

#### IV. CONCLUSIONS

The ECUC has the potential to improve IB solar cell designs. Its maximum detailed balance efficiency is equal to that of a QRSC, and it may be easier to produce. Though DB calculations do not consider nonradiative processes, they give upper bounds on the efficiency of all photovoltaic devices. At low solar concentration, ECUC has a higher limiting efficiency than IBSC. This effect is realized in the c-Si

case at one sun, where an IBSC with non-overlapping absorptions cannot improve on a standard single-gap solar cell, but an ECUC permits significantly improved efficiency. At high concentration, the DB efficiency limits of IBSC, ECUC, and QRSC are close, with a substantial gain compared to a single junction device; the ECUC with  $E_{g2} < E_{g1}$  provides the highest efficiency. Moving beyond DB, the ECUC architecture is designed to allow improved efficiency even with materials having significant nonradiative recombination. It is thus a promising architecture to pursue for near-term development of IB-based devices. The case of a-Si on c-Si provides a promising platform for developing an ECUC with the potential to significantly improve silicon-based solar cell efficiencies.

## ACKNOWLEDGMENTS

We acknowledge helpful conversations with Daniel MacDonald and Wenjie Yang and support from the Natural Sciences and Engineering Research Council of Canada. The data that support the findings of this study are available from the corresponding author upon reasonable request.

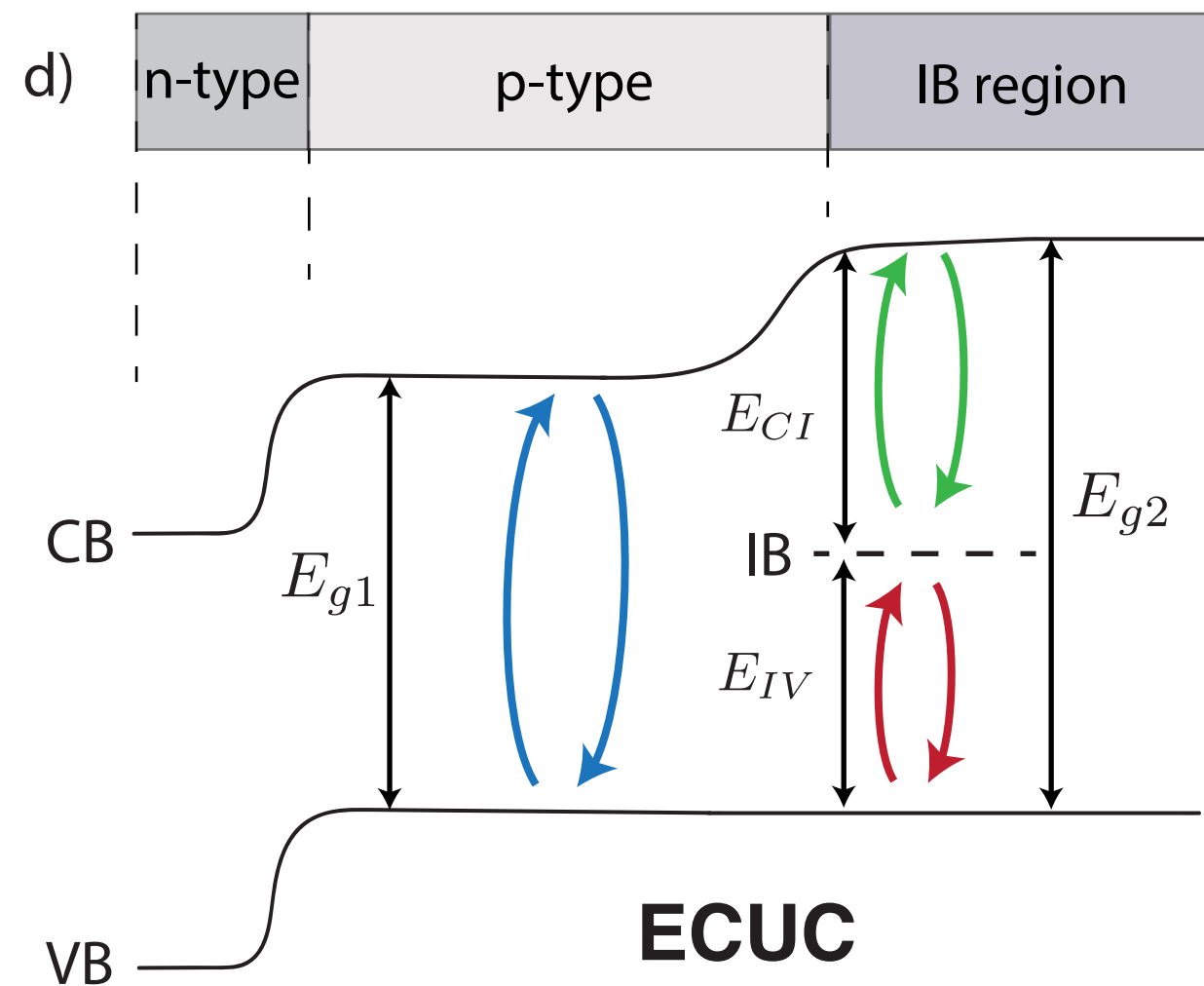
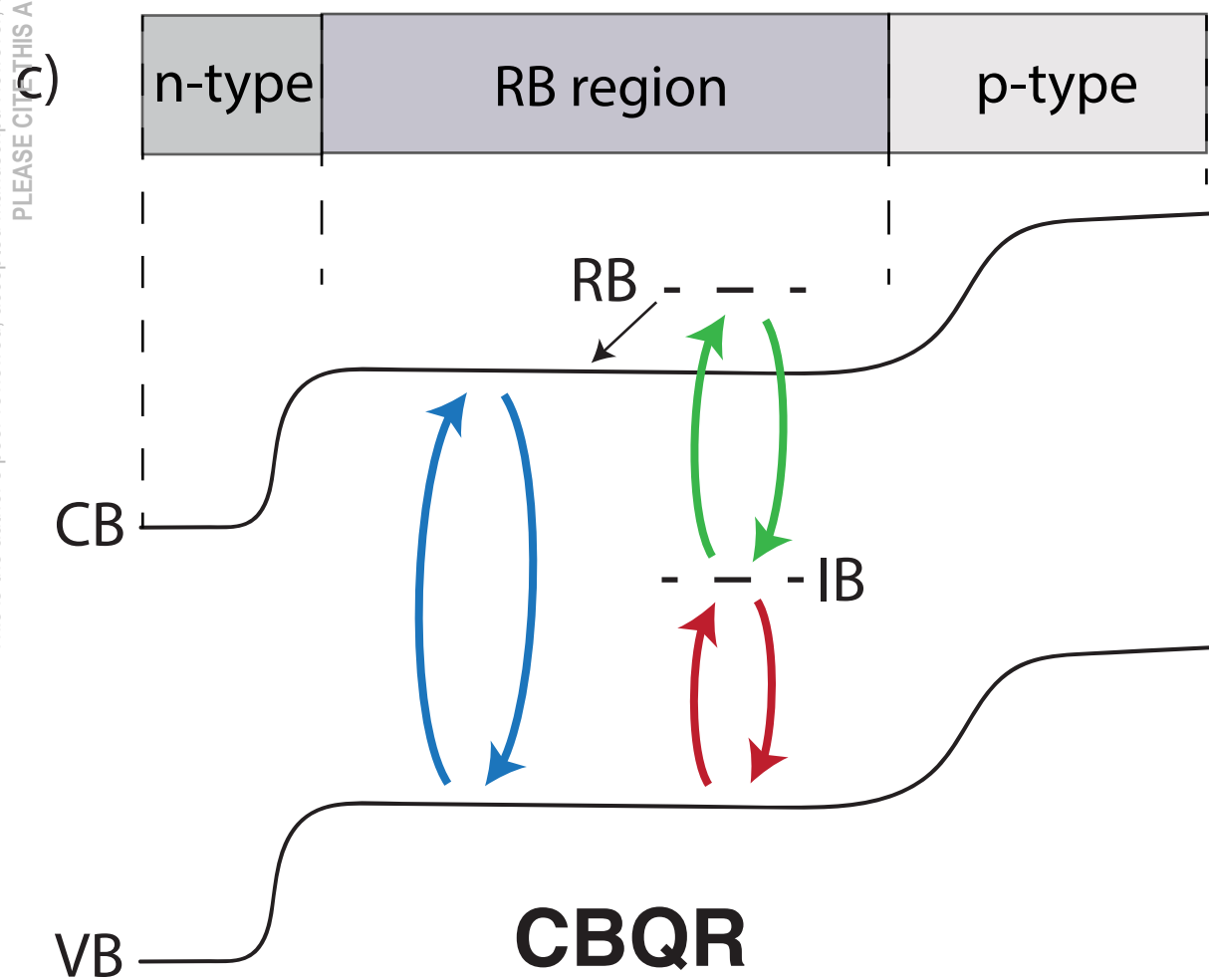
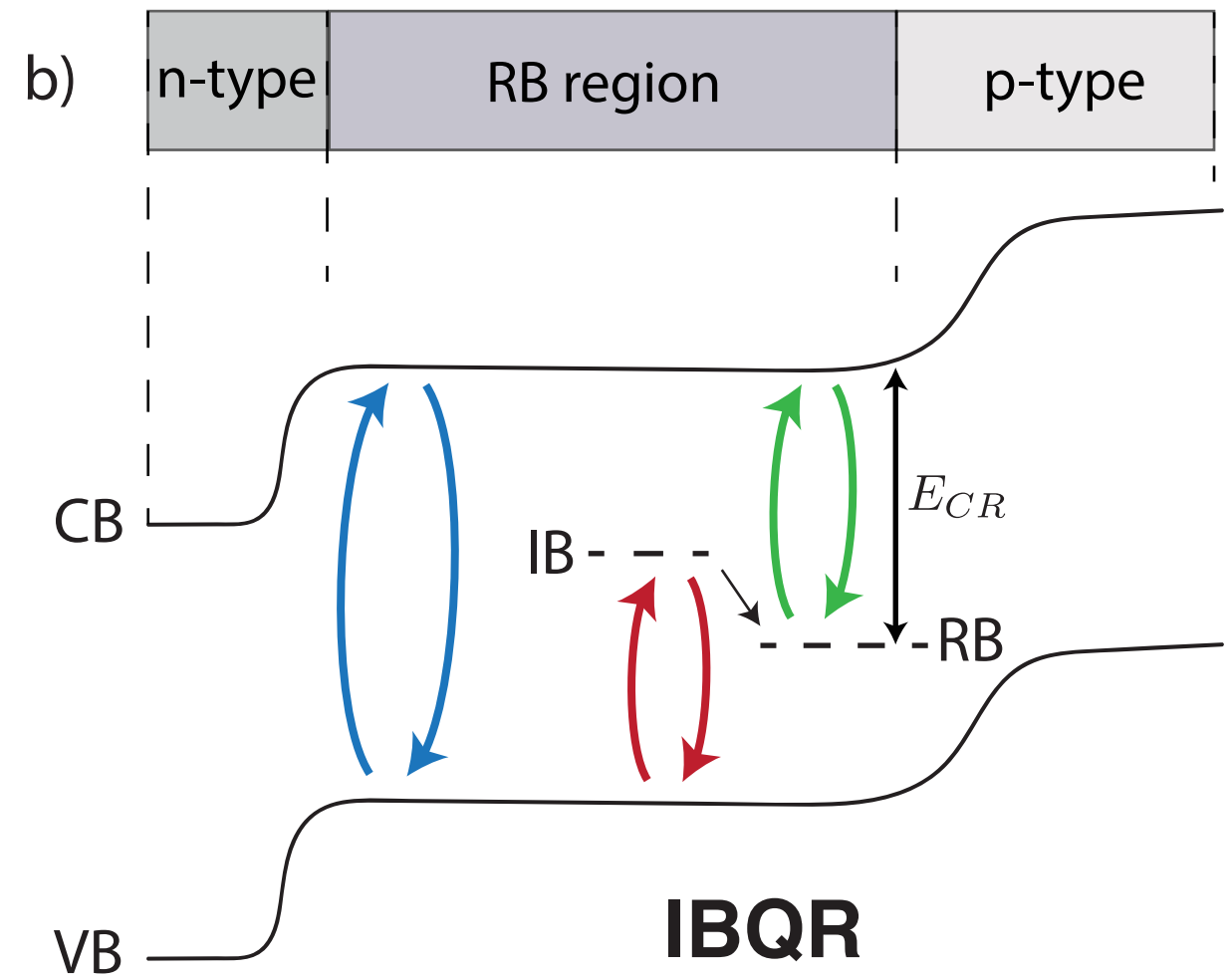
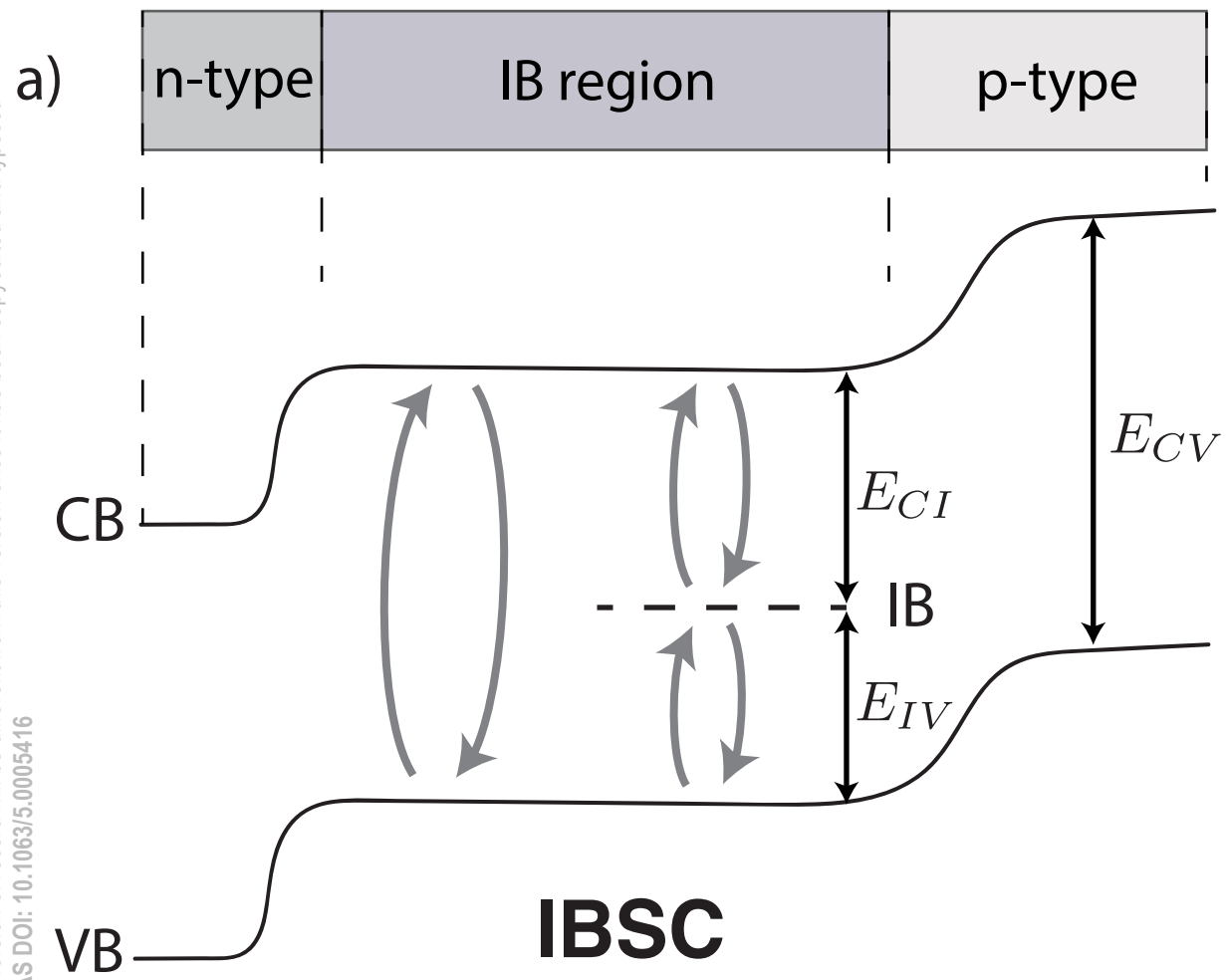
- <sup>1</sup>W. Shockley and H. J. Queisser, "Detailed Balance Limit of Efficiency of p-n Junction Solar Cells," *Journal of Applied Physics* **32**, 510–519 (1961).
- <sup>2</sup>A. Luque and A. Martí, "Increasing the Efficiency of Ideal Solar Cells by Photon Induced Transitions at Intermediate Levels," *Physical Review Letters* **78**, 5014–5017 (1997).
- <sup>3</sup>A. Martí, E. Antolín, C. R. Stanley, C. D. Farmer, N. López, P. Díaz, E. Cánovas, P. G. Linares, and A. Luque, "Production of photocurrent due to intermediate-to-conduction-band transitions: A demonstration of a key operating principle of the intermediate-band solar cell," *Phys. Rev. Lett.* **97**, 247701– (2006).
- <sup>4</sup>W. Wang, A. S. Lin, and J. D. Phillips, "Intermediate-band photovoltaic solar cell based on ZnTe:O," *Appl. Phys. Lett.* **95**, 011103 (2009).
- <sup>5</sup>N. López, L. A. Reichertz, K. M. Yu, K. Campman, and W. Walukiewicz, "Engineering the electronic band structure for multiband solar cells," *Phys. Rev. Lett.* **106**, 028701– (2011).
- <sup>6</sup>Y. Okada, T. Morioka, K. Yoshida, R. Oshima, Y. Shoji, T. Inoue, and T. Kita, "Increase in photocurrent by optical transitions via intermediate quantum states in direct-doped InAs/GaNAs strain-compensated quantum dot solar cell," *J. Appl. Phys.* **109**, 024301–5 (2011).
- <sup>7</sup>N. Ahsan, N. Miyashita, M. M. Islam, K. M. Yu, W. Walukiewicz, and Y. Okada, "Two-photon excitation in an intermediate band solar cell structure," *Appl. Phys. Lett.* **100**, 172111–4 (2012).
- <sup>8</sup>J. T. Sullivan, C. B. Simmons, J. J. Krich, A. J. Akey, D. Recht, M. J. Aziz, and T. Buonassisi, "Methodology for vetting heavily doped semiconductors for intermediate band photovoltaics: A case study in sulfur-hyperdoped silicon," *J. Appl. Phys.* **114**, 103701 (2013).
- <sup>9</sup>S. P. Hill, T. Dilbeck, E. Baduelli, and K. Hanson, "Integrated photon up-conversion solar cell via molecular self-assembled bilayers," *ACS Energy Lett.* **1**, 3–8 (2016).
- <sup>10</sup>H. Hosokawa, R. Tamaki, T. Sawada, A. Okonogi, H. Sato, Y. Ogomi, S. Hayase, Y. Okada, and T. Yano, "Solution-processed intermediate-band solar cells with lead sulfide quantum dots and lead halide perovskites," *Nature Communications* **10**, 43 (2019).
- <sup>11</sup>Y. Okada, N. J. Ekins-Daukes, T. Kita, R. Tamaki, M. Yoshida, A. Pusch, O. Hess, C. C. Phillips, D. J. Farrell, K. Yoshida, N. Ahsan, Y. Shoji, T. Sogabe, and J. F. Guillemoles, "Intermediate band solar cells: Recent progress and future directions," *Applied Physics Reviews* **2**, 021302 (2015).
- <sup>12</sup>M. Yoshida, N. J. Ekins-Daukes, D. J. Farrell, and C. C. Phillips, "Photon ratchet intermediate band solar cells," *Applied Physics Letters* **100**, 3–7 (2012).
- <sup>13</sup>A. Pusch, M. Yoshida, N. P. Hylton, A. Mellor, C. C. Phillips, O. Hess, and N. J. Ekins-Daukes, "Limiting efficiencies for intermediate band solar cells with partial absorptivity: the case for a quantum ratchet," *Progress in Photovoltaics: Research and Applications* **24**, 656–662 (2016).
- <sup>14</sup>A. Pusch and N. J. Ekins-Daukes, "Voltage Matching, Étendue, and Ratchet Steps in Advanced-Concept Solar Cells," *Physical Review Applied* **12**, 044055 (2019).
- <sup>15</sup>A. Vaquero-Stainer, M. Yoshida, N. P. Hylton, A. Pusch, O. Curtin, M. Frogley, T. Wilson, E. Clarke, K. Kennedy, N. J. Ekins-Daukes, O. Hess, and C. C. Phillips, "Semiconductor nanostructure quantum ratchet for high efficiency solar cells," *Communications Physics* **1**, 2–8 (2018).
- <sup>16</sup>J. J. Krich, B. I. Halperin, and A. Aspuru-Guzik, "Nonradiative lifetimes in intermediate band photovoltaics—Absence of lifetime recovery," *Journal of Applied Physics* **112**, 013707 (2012).
- <sup>17</sup>M. M. Wilkins, E. C. Dumitrescu, and J. J. Krich, "Material quality requirements for intermediate band solar cells," *IEEE Journal of Photovoltaics*, *IEEE Journal of Photovoltaics* **10**, 467–474 (2020).
- <sup>18</sup>D. MacDonald, K. McLean, P. N. Deenapanray, S. De Wolf, and J. Schmidt, "Electronically-coupled up-conversion: An alternative approach to impurity photovoltaics in crystalline silicon," *Semiconductor Science and Technology* **23**, 015001 (2008).
- <sup>19</sup>N. P. Harder and D. Macdonald, "Electronic up-conversion: a combination of the advantages of impurity photovoltaics and (optical) up-conversion," *31st IEEE Photovoltaic Specialists Conference*, 110–113 (2005).
- <sup>20</sup>T. Trupke, M. A. Green, and P. Würfel, "Improving solar cell efficiencies by up-conversion of sub-band-gap light," *Journal of Applied Physics* **92**, 4117–4122 (2002).
- <sup>21</sup>A. Krishna and J. J. Krich, "Increasing efficiency in intermediate band solar cells with overlapping absorptions," *Journal of Optics (United Kingdom)* **18**, 074010 (2016).
- <sup>22</sup>L. Cuadra, A. Martí, and A. Luque, "Influence of the overlap between the absorption coefficients on the efficiency of the intermediate band solar cell," *IEEE Transactions on Electron Devices* **51**, 1002–1007 (2004).
- <sup>23</sup>P. Würfel, "The chemical potential of radiation," *Journal of Physics C: Solid State Physics* **15**, 3967–3985 (1982).
- <sup>24</sup>R. Strandberg and T. W. Reenaas, "Limiting efficiency of intermediate band solar cells with spectrally selective reflectors," *Applied Physics Letters* **97**, 031910 (2010).
- <sup>25</sup>A. Luque and A. Martí, "The intermediate band solar cell: Progress toward the realization of an attractive concept," *Advanced Materials* **22**, 160–174 (2010).
- <sup>26</sup>T. Sogabe, Y. Shoji, M. Ohba, K. Yoshida, R. Tamaki, H. F. Hong, C. H. Wu, C. T. Kuo, S. Tomić, and Y. Okada, "Intermediate-band dynamics of quantum dots solar cell in concentrator photovoltaic modules," *Scientific Reports* **4**, 1–7 (2014).
- <sup>27</sup>R. Strandberg, "Analytic *JV*-Characteristics of Ideal Intermediate Band Solar Cells and Solar Cells with Up and Downconverters," *IEEE Transactions on Electron Devices* **64**, 2275–2282 (2017).
- <sup>28</sup>D. E. Carlson and C. R. Wronski, "Amorphous silicon solar cell," *Applied Physics Letters* **28**, 671–673 (1976).
- <sup>29</sup>T. Mishima, M. Taguchi, H. Sakata, and E. Maruyama, "Development status of high-efficiency HIT solar cells," *Solar Energy Materials and Solar Cells* **95**, 18–21 (2011).
- <sup>30</sup>D. E. Carlson, "The doping of hydrogenated amorphous silicon and its impact on devices," *Critical Reviews in Solid State and Materials Sciences* **16**, 417–435 (1990).
- <sup>31</sup>R. A. Street, D. K. Biegelsen, and R. L. Weisfield, "Recombination in a-Si: H: Transitions through defect states," *Physical Review B* **30**, 5861–5870 (1984).
- <sup>32</sup>A. Matsuda, S. Yamasaki, K. Nakagawa, H. Okushi, K. Tanaka, S. Iizima, M. Matsumura, and H. Yamamoto, "Electrical and Structural Properties of Phosphorous-Doped Glow-Discharge Si:F:H and Si:H Films," *Japanese Journal of Applied Physics* **19**, L305–L308 (1980).
- <sup>33</sup>A. H. Mahan, R. C. Kernsa, and G. Devaud, "BF<sub>3</sub>-doped amorphous silicon thin films," *Journal of Electronic Materials* **12**, 1033–1049 (1983).
- <sup>34</sup>P. Le Comber, W. Spear, G. Müller, and S. Kalbitzer, "Electrical and photoconductive properties of ion implanted amorphous silicon," *Journal of Non-Crystalline Solids* **35-36**, 327–332 (1980).
- <sup>35</sup>C. S. Nichols and C. Y. Fong, "Effects of local disorder on donor states in amorphous silicon," *Physical Review B* **35**, 9360–9363 (1987).
- <sup>36</sup>J. T. Sullivan, C. B. Simmons, T. Buonassisi, and J. J. Krich, "Targeted Search for Effective Intermediate Band Solar Cell Materials," *IEEE Journal*

This is the author's peer reviewed, accepted manuscript. However, the online version of record will be different from this version once it has been copyedited and typeset.

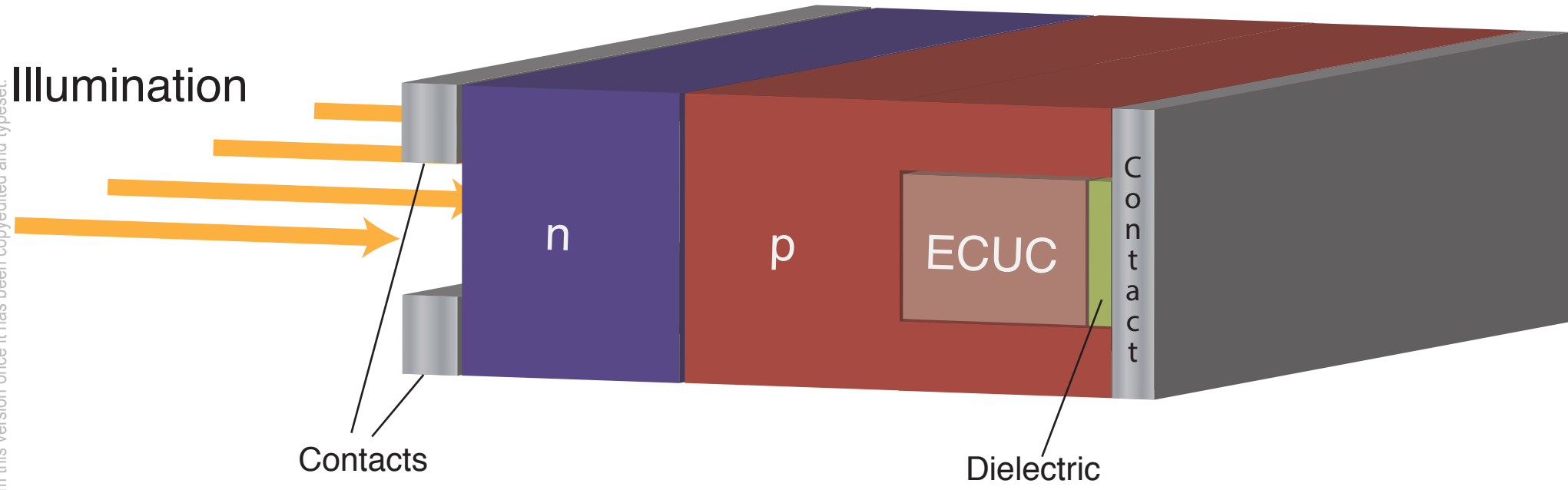
PLEASE CITE THIS ARTICLE AS DOI: 10.1063/1.50005416

of Photovoltaics 5, 212–218 (2015).

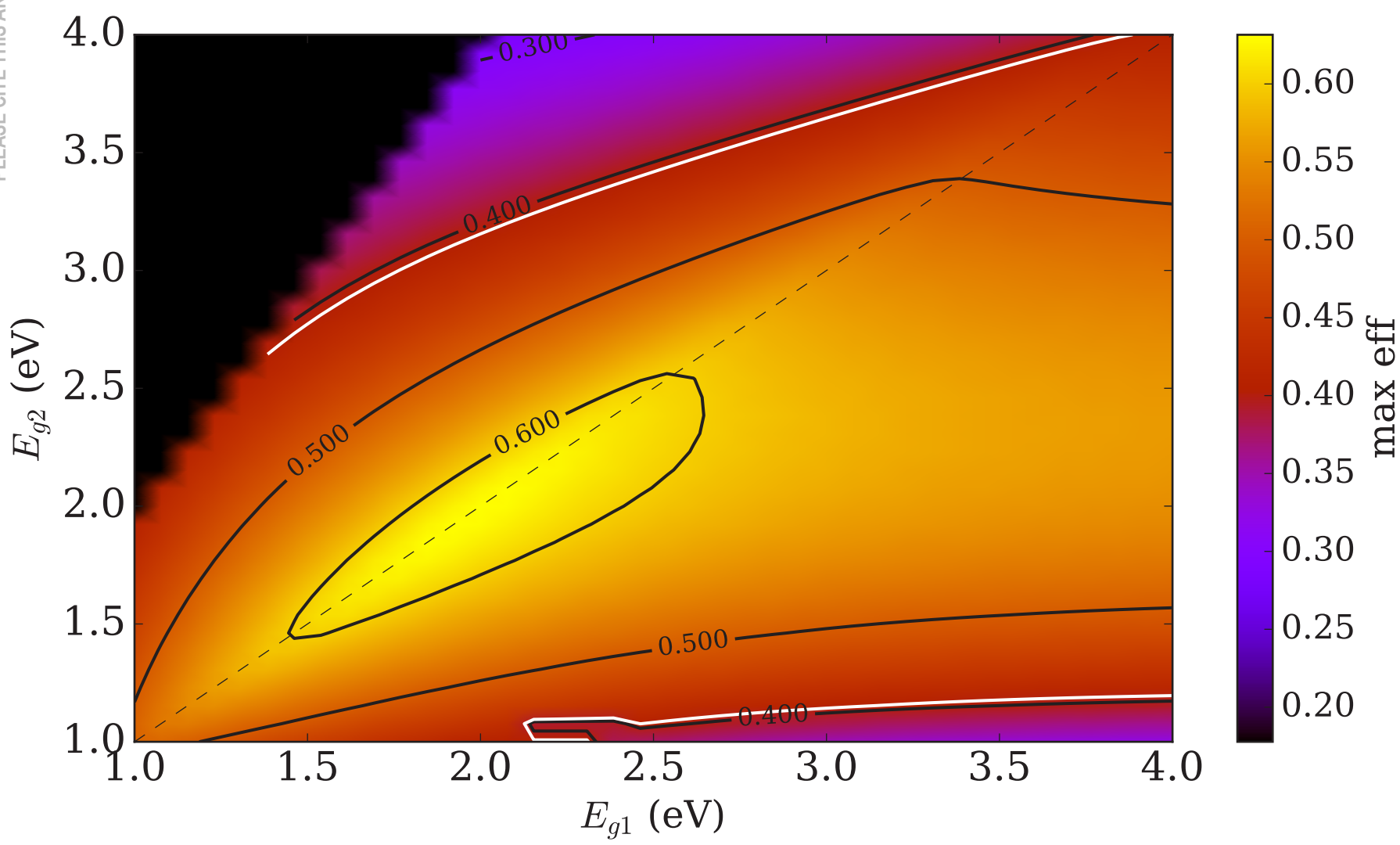
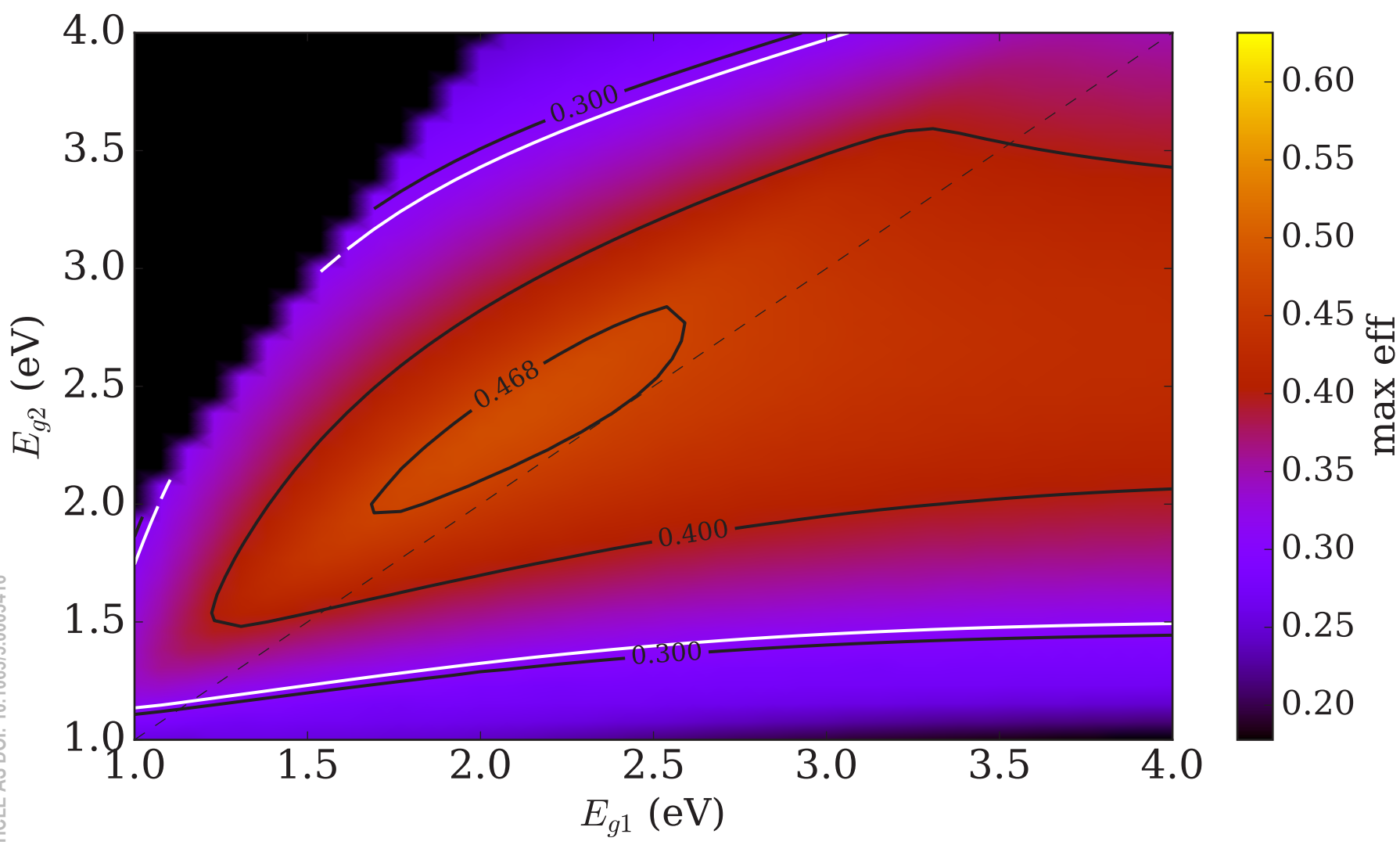
This is the author's peer reviewed, accepted manuscript. However, the online version of record will be different from this version once it has been copyedited and typeset. PLEASE CITE THIS ARTICLE AS DOI: 10.1063/5.0005416



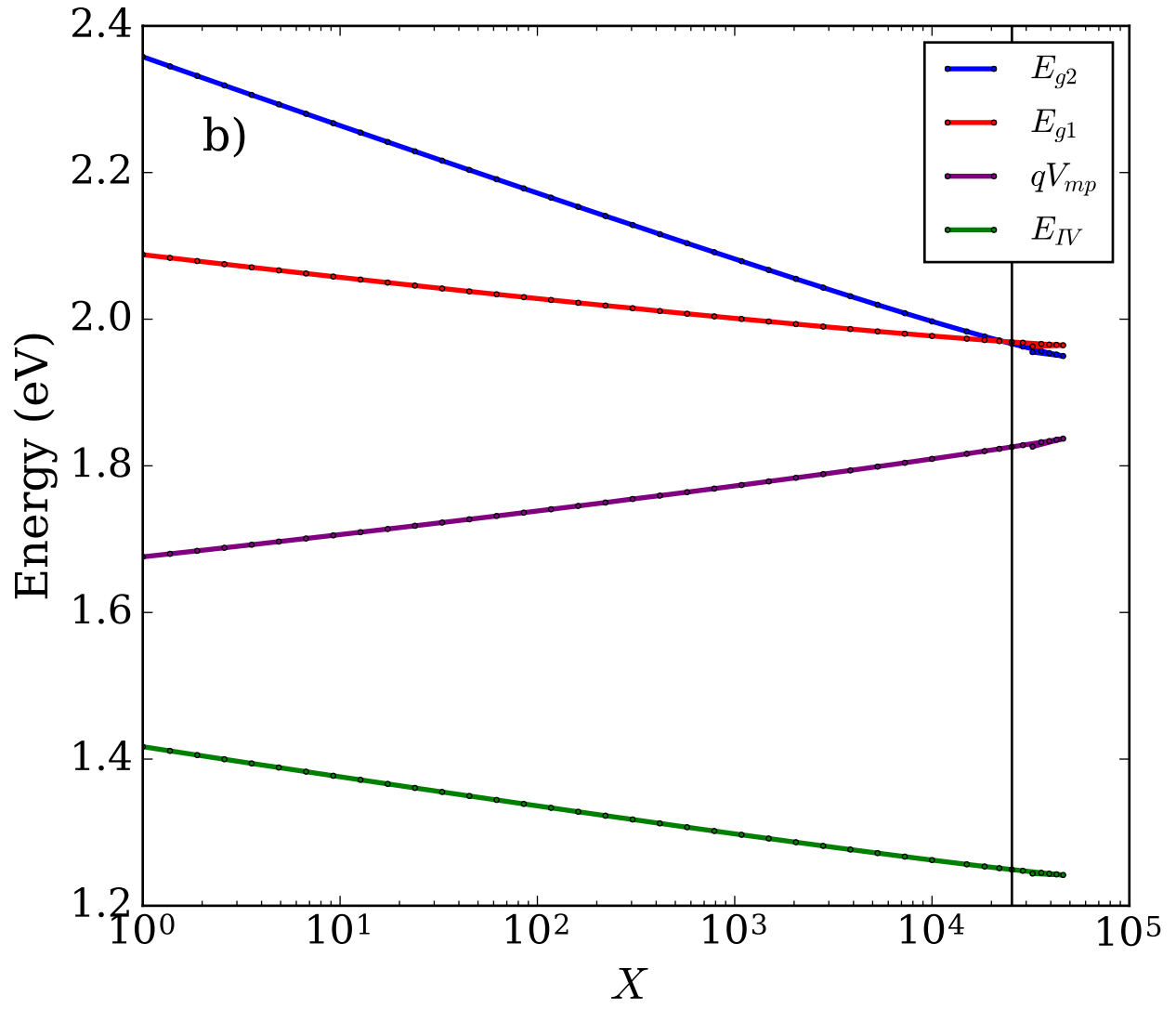
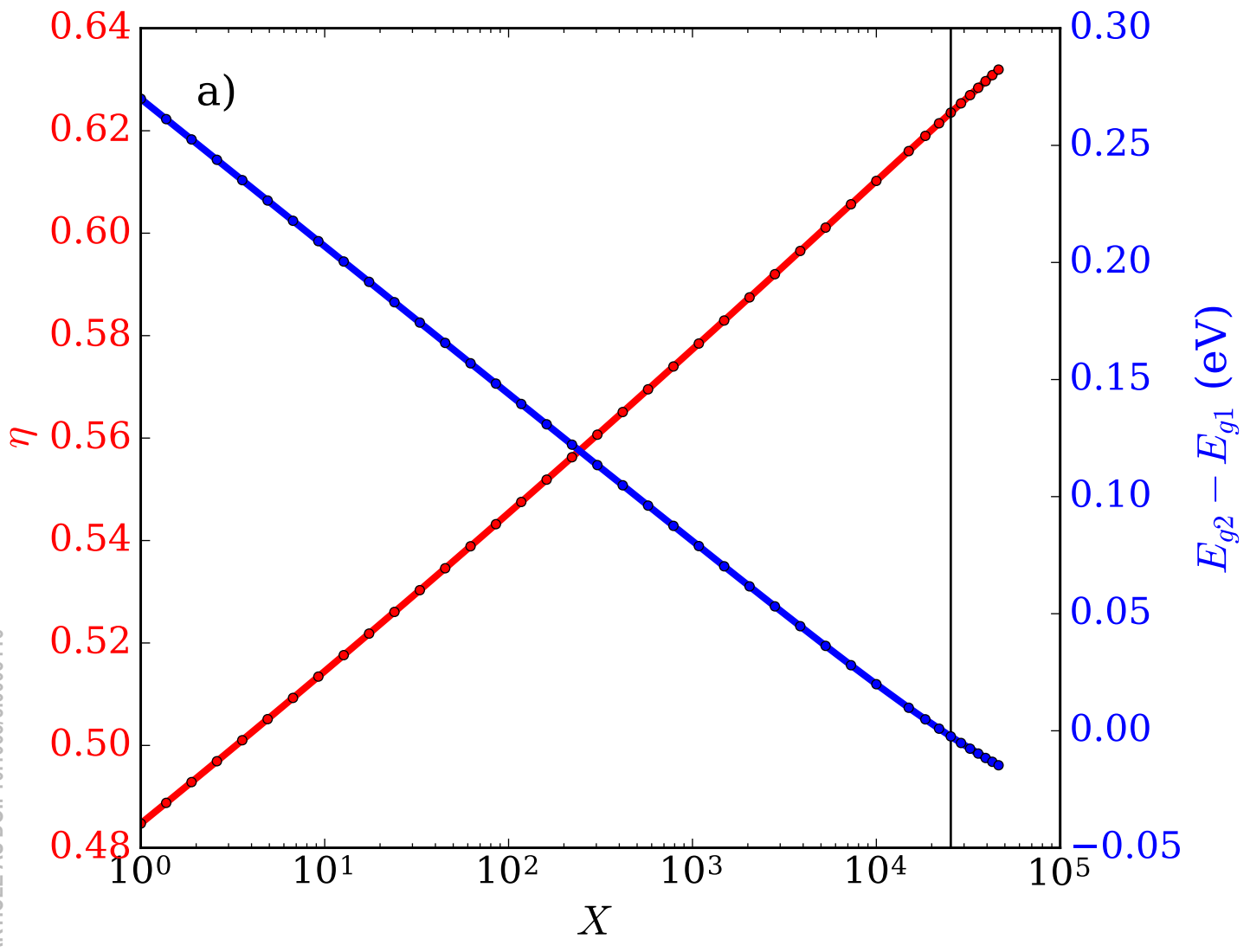
This is the author's peer reviewed, accepted manuscript. However, the online version of record will be different from this version once it has been copyedited and typeset.  
PLEASE CITE THIS ARTICLE AS DOI: 10.1063/5.0005416



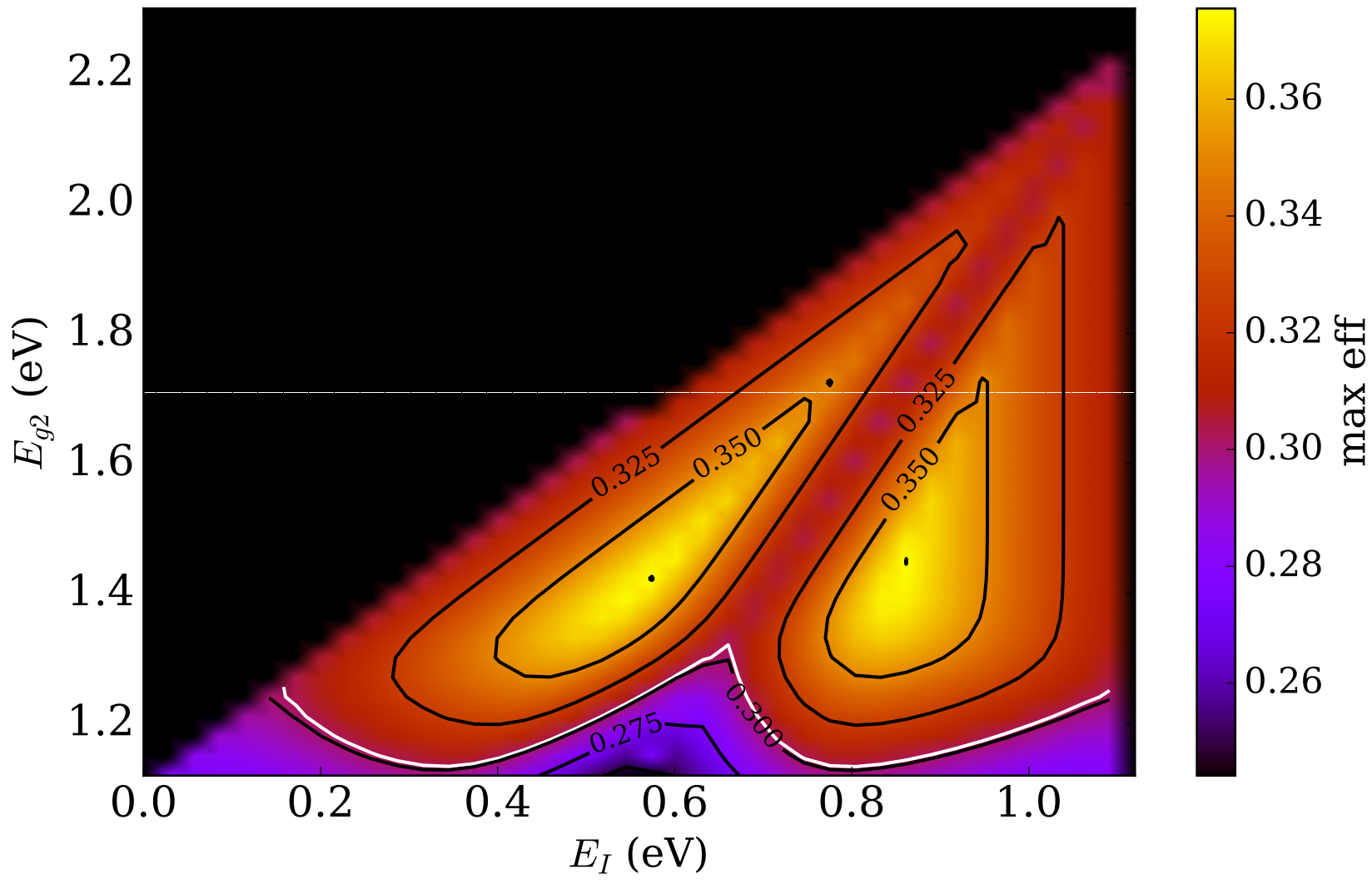
This is the author's peer reviewed, accepted manuscript. However, the online version of record will be different from this version once it has been copyedited and typeset.  
PLEASE CITE THIS ARTICLE AS DOI: 10.1063/1.50005416



This is the author's peer reviewed, accepted manuscript. However, the online version of record will be different from this version once it has been copyedited and typeset.  
PLEASE CITE THIS ARTICLE AS DOI: 10.1063/5.0005416



This is the author's peer reviewed, accepted manuscript. However, the online version of record will be different from this version once it has been copyedited and typeset.  
PLEASE CITE THIS ARTICLE AS DOI: 10.1063/5.0005416



This is the author's peer reviewed, accepted manuscript. However, the online version of record will be different from this version of manuscript. It has been copyedited and typeset.  
PLEASE CITE THIS ARTICLE AS DOI: 10.1063/5.0005416

max eff

